



Removal of crystal violet from aqueous solution using iron based metal organic framework

Sanju Soni^a, Parmendra Kumar Bajpai^b, Dipti Bharti^c, Jyoti Mittal^d, Charu Arora^{a,*}

^aDepartment of Chemistry, Guru Ghasidas University, Bilaspur 495009, India, emails: charuarora150@gmail.com (C. Arora), sanjuser87@gmail.com (S. Soni)

^bDepartment of Pure and Applied Physics, Guru Ghasidas University, Bilaspur 495009, India, email: bajpai.pk1@gmail.com (P.K. Bajpai)

^cDepartment of Chemistry, Greater Noida Institute of Technology, Greater Noida, UP, India, email: dipti1086@gmail.com (D. Bharti)

^dDepartment of Chemistry, Maulana Azad National Institute of Technology, Bhopal, India, email: jyalmittal@yahoo.co.in (J. Mittal)

Received 24 June 2019; Accepted 25 July 2020

ABSTRACT

Iron-benzene dicarboxylic acid (BDC) metal-organic framework (MOF) has been synthesized by solvothermal method at room temperature and tested for the adsorptive removal of the organic dye crystal violet from aqueous solution. Dye removal efficiency and adsorption characteristics were determined to investigate factors such as the effect of dye concentration, contact time, temperature, dose, and pH. Maximum dye removal efficiency was recorded to be 100% with an initial dye concentration of 5 mg/L. Langmuir, Freundlich, and Temkin adsorption isotherm models were used to investigate the adsorption process. The adsorption isotherm of crystal violet onto Fe-BDC-MOF can be described by Freundlich isotherm model and Langmuir isotherm model. Pseudo-second-order kinetic model with rate constant 1.22×10^{-2} g/mg.min is found to be the best fit for the adsorption. Thermodynamic parameters viz. free energy; enthalpy, and entropy have been calculated with the help of adsorption isotherm data. The values of enthalpy and entropy have been obtained as 0.0947 kJ/mol and 0.325 kJ/mol/K, respectively, indicating an endothermic process with an increase in randomness at the solid-solution interface during adsorption. Negative value of ΔG illustrates the process to be spontaneous. Column adsorption capacity of Fe-BDC-MOF has been recorded 26.65 mg/g.

Keywords: MOF; Crystal violet; Adsorption; Kinetics; Thermodynamics

1. Introduction

Synthetic dye effluents, used in different industries such as plastic, paper, and textile, etc., are introduced in water resources as waste and most of these organic dyes are toxic, inert, non-biodegradable, and can cause cancer. Therefore, removing color from these wastes has been increasing scientific interest in the last few decades [1–4]. Several physico-chemical methods such as sedimentation, filtration, radiation treatment, electrochemical treatment, photochemical method, biodegradation, chemical oxidation, coagulation,

reverse osmosis, flotation, and adsorption, etc. have been used to decolorize waste dye effluents [5,6]. As adsorption is a cheap, convenient, and effective method, so it is most preferred and widely used among all methods [2]. In the last few years several materials like wood, coal, clay, crushed brick, saw dust, activated carbon, graphene based materials, chitosan composite, nanohybrid composite, nanomaterials, and other porous materials have been reported to remove dyes from wastewater [1,2,5–14]. Porous metal organic frameworks (MOFs) can be potential adsorbent for the removal of organic dyes from industrial effluents due to their adsorptive

* Corresponding author.

properties. MOFs are crystalline materials that have gained great attention from both academia and industries. MOFs, which are composed of metal ions or clusters bridged by organic linkers having a greater surface area with an advantage of tunable pore sizes, are gaining attention for the potential for vast applications like gas storage, adsorption, separation, drug delivery, catalysis, sensing, photoluminescence, and analytical chemistry because of their versatile physical and chemical properties like controllable pore volume, high surface area, multiple functionalities, etc. [15–17]. In recent years adsorption removal of pollutants from industrial waste using MOFs has attracted attention. There are several reports on the application of MOFs like Ti-MIL-125 [18], Zn-MOF [19], Cr-MIL-53, Cr-MIL-101 [20], Fe-MOF-235 [21], and many more [22–27] which are used as an adsorbent for dye effluents. There are few reports on the removal of crystal violet using MOFs [28–31]. Fe-BDC MOF has been explored for the first time for adsorptive removal of crystal violet dye in the present investigation. Use of Fe-BDC MOF in present investigation is recommended due to low cost, ease of synthesis (using solvothermal method, not requiring expensive instruments/laboratory equipments). The adsorbent can be recovered and reused upto five cycles efficiently. Dye can also be recovered and reused as raw material for industries. So, this method is convenient, environment friendly, and economic. This method does not involve the formation of any toxic by-products. On the other hand methods, like photocatalytic degradation [32–37], advanced oxidation processes (AOPs) [38,39], and catalytic degradation [36,37] are relatively costlier as there is a requirement of expensive semiconductor catalytic materials viz. TiO_2 and costly laboratory equipments. Moreover, there are chances of formation of toxic by-products which make the process complicated and expensive [1,9].

Crystal violet (CV) is a cationic dye and belongs to class of triarylmethane dyes. It is used as coloring agent in textile, paper, leather, additives, ink, cosmetics, and analytical chemistry/biochemistry and as pH indicator. Due to its toxic nature, it can cause irritation in eyes, skin and digestive tract, and permanent injury to cornea and conjunctiva. In the extreme condition it may lead to respiratory and kidney failure and permanent blindness. Discharge of the water containing this dye into water bodies can cause environmental degradation and the dye is reduced to leuco moiety, leucocrystal violet [40–42]. The concentration of dyes in industrial effluents lies in the range of 1–100 mg/L in textile industries waste. As a matter of fact concentration of CV in real effluents varies with usage and utility of the dye in a particular industry. We have carried out our investigation in the range of 5–100 mg/L. The suggested method is indeed a highly versatile method and would be fit on large variations of concentrations of the dye CV.

Therefore, the evaluation of removal and adsorption capacity of crystal violet dye using iron based MOF Fe-BDC (BDC – benzene dicarboxylic acid or terephthalic acid) MOF has been carried out. The rates and mechanism of the adsorption process were investigated. The objective of the present study is to explore the application of Fe-BDC MOF as potential adsorbent for removal of crystal violet and to study the effect of contact time, initial concentration, pH, amount of the adsorbent, and temperature on the adsorption process.

2. Experimental

2.1. Materials and method

For the present study, commercially available chemical and reagents were used without any further purification. Shimadzu UV 1800 spectrophotometer (Kyoto, Japan) having a 10 mm quartz cuvette was used to record UV-vis spectra of dye solutions in the visible range in the absorbance mode. Scanning electron microscopy (SEM) micrographs of the samples before and after adsorption were captured using Merlin VP compact (Carl ZEISS Germany make), Jena, Germany having an air lock chamber. To determine the crystal morphology transmission electron microscopy (TEM) images were recorded using a JEOL JEM-2100F microscope (Tokyo, Japan) at 200 kV operational mode. TEM samples were prepared by drop-casting a dilute solution in dimethyl sulfoxide (0.5 mg/mL) on a carbon coated Cu-grid and the drying this at 50°C for 12 h in vacuum oven. Surface area and pore volume of the adsorbent Fe-BDC MOF were determined using Brunauer–Emmett–Teller (BET) method (Sorptomatic 1990) after degassing at 110°C under vacuum, using nitrogen adsorption at –196°C and desorption while allowing the temperature to rise to ambient. Zeta potential of the adsorbent was determined by using zeta-sizer Nano-ZS (Malvern) instrument.

2.2. Synthesis of the adsorbent and adsorption study

The MOF Fe-BDC was synthesized and characterized as per our previously published article [43]. Removal of CV dye was investigated spectrophotometrically. A stock solution (100 mg/L) of CV dye was prepared by dissolving 10 mg of the dye in 100 mL of distilled water. All other subsequent solutions were prepared by diluting the stock solution. For adsorption experiments, a fixed amount of the Fe-BDC MOF (0.03 g) was added to a series of 10 mL diluted solutions (1–6 mg/L) of CV dye, and the difference in the dye concentration was measured at maximum wavelength of CV dye ($\lambda_{\text{max}} = 589 \text{ nm}$). The removal efficiency (%) and the amount of dye adsorbed at equilibrium Q_e (mg/g) were calculated using earlier reported methods [43].

Similar procedure is applied for kinetic study using the solution of dye having 5 mg/L concentration. The aqueous samples were taken to preset time intervals and the concentrations of dye were measured. The amount of dye adsorbed at time t , Q_t (mg/g), was calculated using the Eq. (1):

$$Q_t = \frac{(C_0 - C_t)V}{m} \quad (1)$$

2.3. Effect of initial dye concentration

0.1 g Fe-BDC MOF adsorbent was added to each 10 mL CV dye solutions having initial concentrations 5, 10, 20, 30, 40, 50, 60, 70, 80, 90, and 100 mg/L and the experiments were carried out for 24 h. The concentration of dyes in industrial effluents lies in the range of 10–100 mg/L so most researchers have carried out their studies in the range of 2–100 mg/L [37,40,44–48]. As a matter of fact concentration of CV in real effluents varies with usage and utility of the dye in a particular industry. However, a concentration greater than 100 mg/L leads to losses to industries.

2.4. Effect of contact time

To 10 mL CV dye solution having initial concentration 5 mg/L, 0.03 g of the adsorbent was added and the aqueous samples were taken after time interval of 60, 120, 180, 240, 300, and 1,440 min.

2.5. Effect of adsorbent dose

To study the effect of adsorbent dose on adsorption 15, 20, 25, 30, and 35 mg of Fe-BDC MOF were added to 10 mL solution of CV dye having initial concentration 5 mg/L for 24 h.

2.6. Effect of temperature

Experiment for effect of temperature on adsorption process was carried out at temperature 298, 303, 308, 313, 318, and 323 K for 5 h by adding 0.03 g of adsorbent to 10 mL aqueous solution of CV with initial concentration 5 mg/L.

2.7. Effect of pH

Investigation of effect of solution pH was performed at pH 4, 5, 6, 7, 8, and 9. 0.03 g adsorbent was added to each 10 mL aqueous solution of CV having an initial concentration of 5 mg/L for a constant adsorption time of 24 h. pH of dye solution was adjusted by adding dilute solutions of HCl and NaOH.

2.8. Column adsorption study

Adsorption using column is one of the most common and efficient way for removal of pollutants from water. To decide the amount of adsorbent which is required for removal of pollutants from wastewater, column technique plays an important role [49]. For column adsorption study, 0.25 g of adsorbent was filled in a glass column of 18 cm length and 1 cm internal diameter over the support of cotton wool. The length and cross-section area of the adsorbent bed was 0.3 cm and 0.8 cm², respectively. Through this bed aqueous solution of CV dye was allowed to run downwards and aqueous solutions were analyzed for CV dye concentration after time to time. The column run was stopped as the effluent dye concentration was reached to 90% of influent dye concentration and the breakthrough curve [43] is plotted.

2.9. Dye desorption and reusability

Desorption of adsorbed CV dye was carried by sonicating the used Fe-BDC MOF in acetone for 15 min. The desorbed Fe-BDC MOF sample was reused for CV dye removal study after drying in a hot air oven at 40°C.

3. Results and discussion

3.1. Characterization of Fe-BDC MOF adsorbent

The powder X-ray diffraction (PXRD) pattern (Fig. 1) was recorded after annealing at 120°C for 4 h of as-synthesized Fe-BDC MOF at room temperature. The X-ray diffraction pattern matches with International Centre for Diffraction

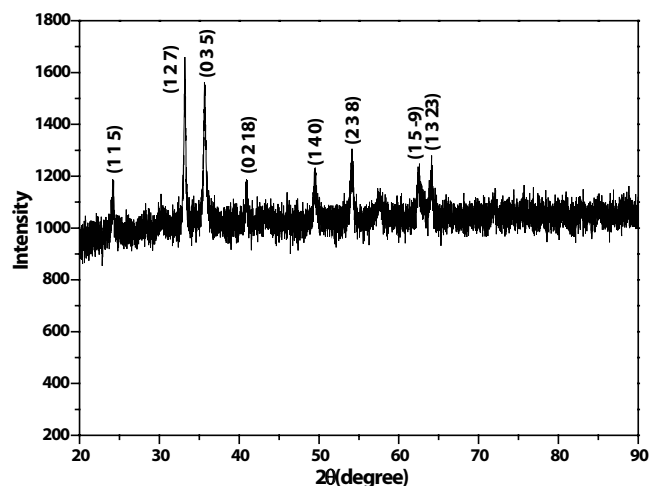


Fig. 1. PXRD of Fe-BDC.

Data file number (PDF-4+2014RDB) DB card number 00–055–1809. Rietveld refinement was implemented using PDXL software, with pseudo-voigt band profile after background correction. After Rietveld refinement of the pattern it reveals monoclinic phase with space group P_12_1/C_1 and cell parameters $a = 5.929 \text{ \AA}$, $b = 7.802 \text{ \AA}$, $c = 51.30 \text{ \AA}$, and $\beta = 110.84^\circ$ having refinement parameters $R_{wp} = 3.65$, $R_p = 2.84$, $R_e = 3.18$, $S = 1.1485$, and $\chi^2 = 1.3191$. Reliability of data is checked by goodness of fitting. The refinement results are shown in Fig. 2.

The Fourier-transform infrared (FT-IR) spectrum of MOF before and after adsorption is shown in (Fig. 3). The observed bands in IR spectrum were used to characterize the material. IR band at 750 cm⁻¹ could be assigned due to benzene ring deformation mode. The broad absorption at $\approx 3,400$ and $\approx 1,300$ cm⁻¹ indicated that water and/or other gases have been adsorbed in the frameworks. Similar observations for some other MOFs have been reported by Tan et al. [50]. Red shift of C–H bending frequency from 1,017 cm⁻¹ indicates occurrence of hydrolysis reaction with Fe–C–O due to exposure of moisture present in the atmosphere. IR signal at 1,394 and 1,101 cm⁻¹ are assigned to C–O stretching and in plane O–H deformation. Broad peak at $\approx 3,400$ cm⁻¹ was due to surface-sorbed water. Peak at 1,589 cm⁻¹ could be assigned for C=O bond stretching vibrations in BDC [51]. Further, peak at 549 cm⁻¹ indicates the presence of strong Fe–O vibration band [52]. The observed vibrational bands suggest the formation of phase pure MOF without impurity within the detection limit of spectroscopy. Appearance of new peaks at 1,573; 1,377; and 1,307 cm⁻¹ after adsorption of dye can be attributed to –C=C–, –C=N–, and –C–N– stretching in polyheterocycles. These bands could be used as evidence for the adsorption of the dyes on MOF.

TEM image of synthesized Fe-BDC MOF is shown in Fig. 4. TEM image reveals particle size of MOF to be 10 nm. BET surface area and pore volume were determined by the use of standard procedures to be 46.02 m²/g and 0.076 cm³/g, respectively.

Figs. 5 and 6 reveal SEM micrographs of Fe-BDC MOF before and after adsorption respectively along with their energy-dispersive X-ray spectroscopy (EDX). Fig. 5 exhibits

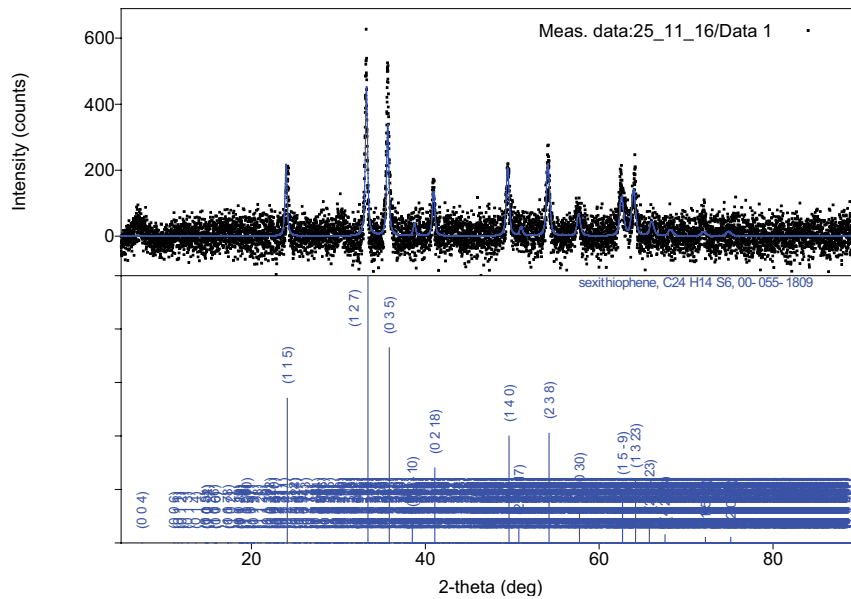


Fig. 2. Rietveld refinement fitting of PXRD of Fe-BDC.

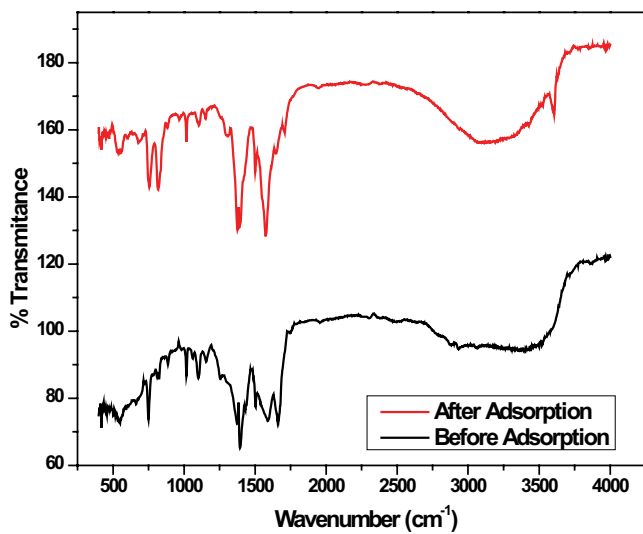


Fig. 3. IR spectrum of Fe-BDC before and after adsorption of Crystal violet.

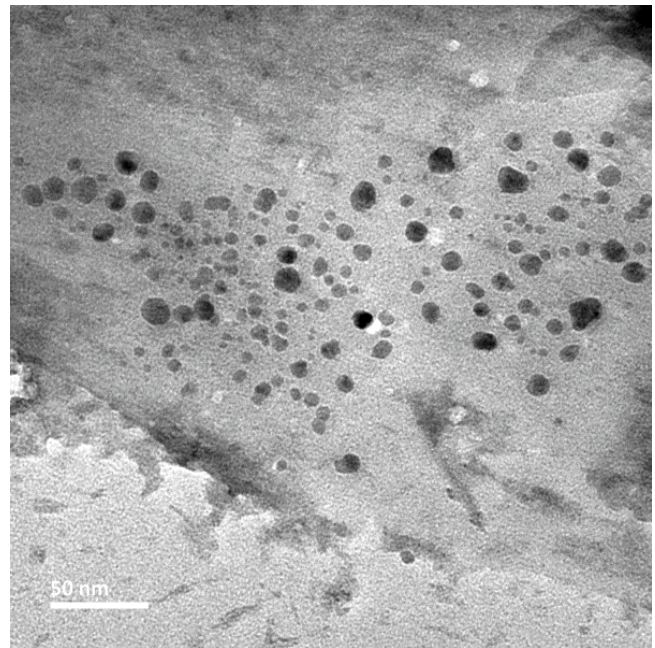


Fig. 4. TEM image of Fe-MOF.

a porous surface of MOF which may be a probable reason for the adsorption of dye molecule. Fig. 6 (SEM images after adsorption) depicts the adsorption of dye molecules on the surface of MOFs. In addition, EDX data before and after adsorption further confirms the adsorption process (Table 1).

3.2. Effect of initial dye concentration

Fig. 7 shows the effect of initial dye concentration on adsorption by Fe-MOF. Concentration range of 5–100 mg/L with an adsorbent dose of 0.1 g has been selected for adsorption experiments. From the figure, it is clear that as the initial dye concentration increases from 5 to 100 mg/L, the percentage of dye removal decreased from 100 to

92.86%. These observations indicate the saturation of binding sites on the surface of adsorbent with increase in dye concentration [53]. Similar observations have been reported for removal of basic dyes [54] as well as crystal violet [55].

3.3. Effect of contact time

Variation of dye removal (%) and adsorption capacity (mg/g) with adsorption time is shown in Figs. 8a and b, respectively. The extent of removal of CV dye increased on increasing contact time. Twenty-four hours is considered

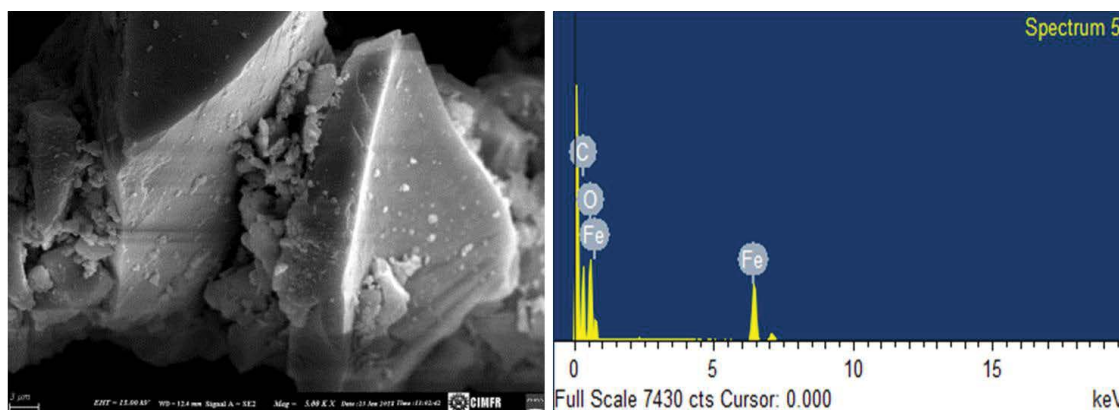


Fig. 5. SEM image and EDX of Fe-MOF before adsorption.

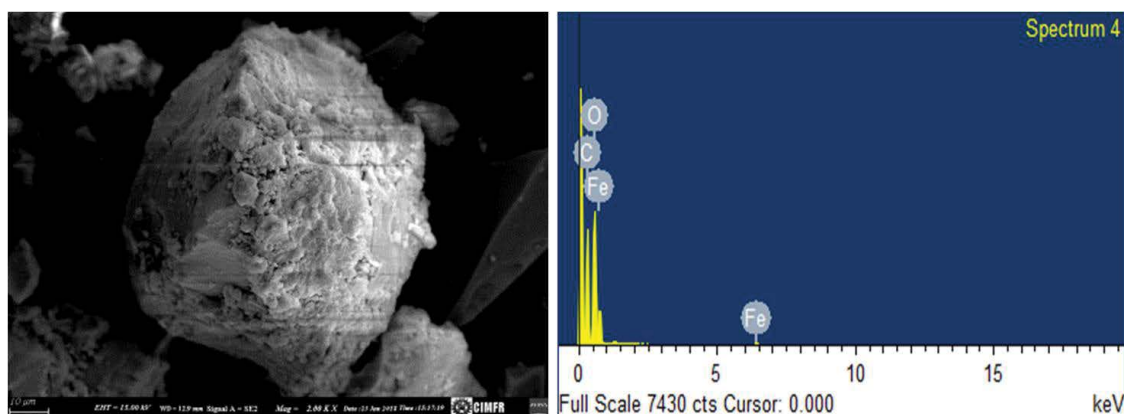


Fig. 6. SEM image and EDX of Fe-MOF after adsorption.

Table 1
Elemental composition of Fe-BDC MOF before and after adsorption

S. No.	Name of elements	Weight percentage of elements (%)	
		Before adsorption	After adsorption
1	Carbon	8.70	12.31
2	Oxygen	40.82	82.83
3	Iron	50.48	4.86

as equilibrium time for this study. It was observed that initially the rate of adsorption of CV dye was high which gradually slows down with time. Initially, large numbers of vacant sites are available at the surface of adsorbent which decreases with time as adsorption of dye molecules takes place. Therefore, less number of vacant sites is available for adsorption of CV as time passes. There may be a possibility of arising repulsive force between the CV dye molecules getting adsorbed on the surface of adsorbent and the CV dye molecules present in solution phase resulting in decrease in adsorption rate [56].

3.4. Effect of adsorbent dose

Effect of adsorbent dose on removal of CV dye is shown in Fig. 9. It was observed that the removal of crystal violet

dye increased with the increase in amount of Fe-BDC MOF. The removal of dye increased from 43.75% to 93.46% with an increase in the amount of MOF from 15 to 35 mg due to increased surface area and adsorption sites [57].

3.5. Effect of temperature

The effect of temperature on the adsorption of CV on Fe-BDC MOF was carried out at 298, 303, 308, 313, 318, and 323 K for 5 h. When the temperature is increased there is an increase in the rate of diffusion of the dye molecules across the external boundary layer which decreases the viscosity of the solution. As a result equilibrium capacity of the adsorbent for a particular adsorbate varies on changing temperature [58]. In the present study, adsorption capacity increased from 1.47 to 1.66 mg/g, and dye removal is

increased from 88.5% to 99.35% when the temperature of the dye solution was increased from 298 to 323 K (Fig. 10) which indicates the adsorption process to be endothermic [58].

3.6. Effect of pH

Effect of solution pH on the adsorption process is represented in Fig. 11. Maximum dye uptake was observed at pH 6. In general, for cationic dyes, on increasing initial pH there is a tendency of increase in adsorption capacity due to an increase in electrostatic interaction between negatively charged surface of adsorbent and cationic dye molecules. The increase in the extent of adsorption with an increase in pH value is due to the neutralization of the charges at the surface of the adsorbent. It can be safely assumed that by increasing the pH of the solution preference of

the negative centers of the dye for the active sites of the adsorbent increases, which in turn facilitates the adsorption process. However, beyond pH 6 with increase in alkaline conditions protonation of the dye is reduced, and electrostatic repulsion between OH^- adsorbed on the adsorbent and ionized dye molecule retards the extent of diffusion and adsorption thereby. A similar result has been reported by Prasad and Santhi [41].

The surface charge of the MOF adsorbent was investigated by determining its zero point charge (pH_{zpc}). As shown in Fig. 11, the pH_{zpc} for the Fe-BDC MOF is 4.9 and the adsorbent has positive zeta potential at lower pH indicating the positive surface charge which turns negative as the pH increases, that is, negative zeta potential. At higher pH ranges the adsorbent surface carries negative charge which benefits the adsorption of cationic CV dye through electrostatic interaction. Therefore, adsorption rate were improved with increasing pH values from 4 to 6. When pH value was higher than 6, the adsorption rate of Fe-BDC MOF for CV dye decreased with further increasing pH values. This can be ascribed to the hydrogen bond interaction between cationic CV dye and Fe-BDC MOF which is stronger than that of the electrostatic interaction [59].

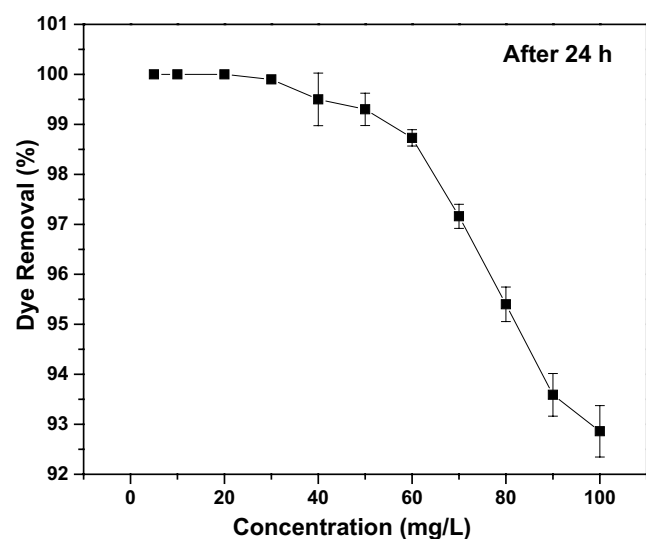


Fig. 7. Effect of initial concentration of dye (Fe-BDC = 0.1 g, equilibrium time = 24 h, and volume of dye solution = 10 mL).

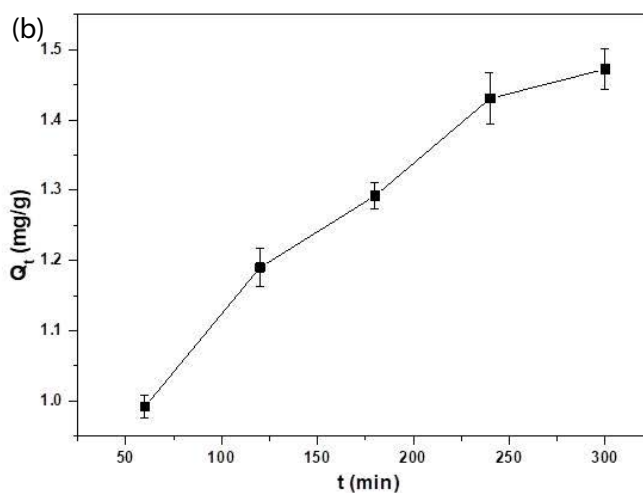
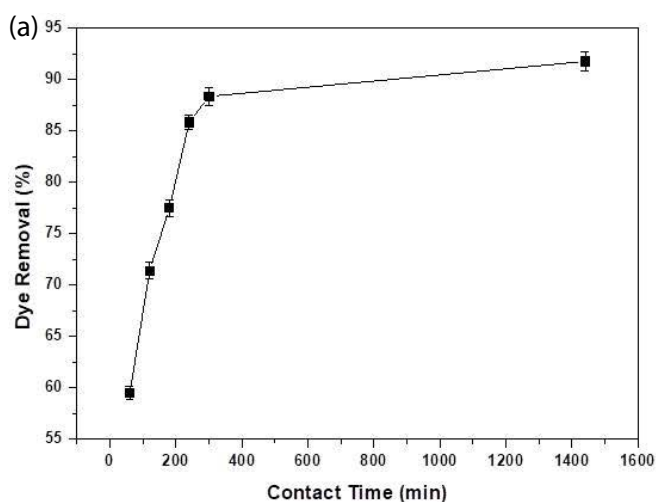


Fig. 8. Effect of contact time on (a) dye removal and (b) on adsorption capacity (Fe-BDC MOF = 0.03 g, initial concentration of dye = 5 mg/L, and volume of dye solution = 10 mL).

3.7. Adsorption equilibrium

At equilibrium, distribution of dye molecules between the two phases, that is, solid phase and liquid phase is suggested by the adsorption isotherms. Interaction between the dye molecules and the adsorbent surface can be explained by analysis of the isotherm data by fitting them to different isotherm models. The isotherm data were fitted to Freundlich, Langmuir, and Temkin isotherms.

3.7.1. Freundlich adsorption isotherm

Freundlich model explains adsorption on heterogeneous surface with non-uniform distribution of heat of adsorption. It assumes that there is an interaction between adsorbed

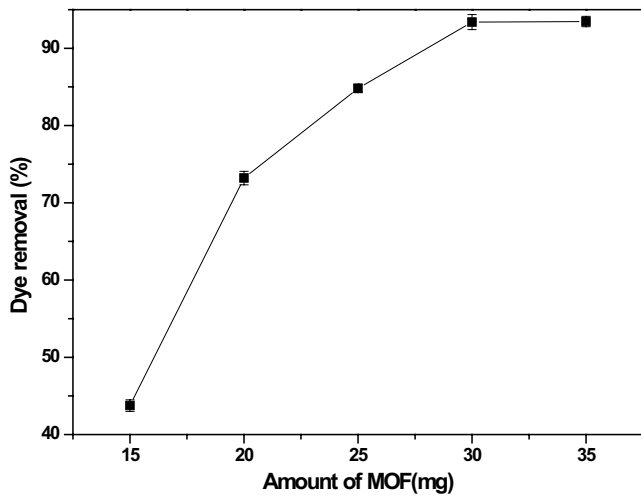


Fig. 9. Effect of amount of MOF on dye removal (initial concentration of dye = 5 mg/L, volume = 10 mL, and contact time = 24 h).

molecules [45,57]. The Freundlich adsorption isotherm is represented by the following linear equation:

$$\ln Q_e = \ln K_F + \frac{1}{n} \ln C_e \quad (2)$$

Here, C_e is the equilibrium concentration (mg/L) of CV, Q_e adsorption capacity (mg/g), and K_F and n are the Freundlich constants related to the adsorption capacity and adsorption intensity, respectively. Value of constant n provides information about how favorable is the adsorption process. If the value of $1/n$ is closer to 0, adsorption becomes more heterogeneous [58].

3.7.2. Langmuir adsorption isotherm

Linear form of Langmuir isotherm [60] is given as:

$$\frac{C_e}{Q_e} = \frac{C_e}{Q_L} + \frac{1}{K_L Q_L} \quad (3)$$

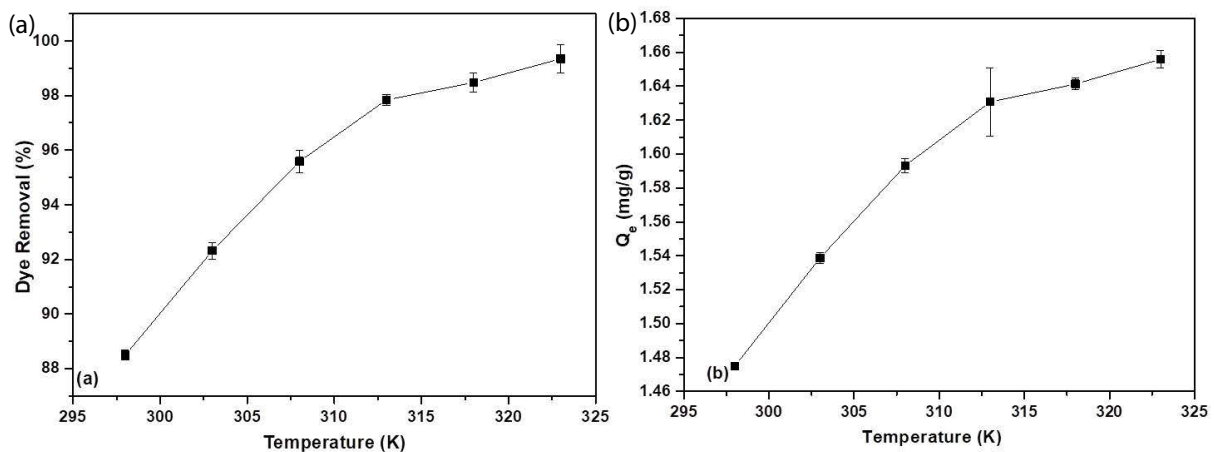


Fig. 10. Effect of temperature on (a) dye removal and (b) equilibrium capacity (initial concentration of dye = 5 mg/L, amount of MOF = 0.03 g, and contact time = 24 h).

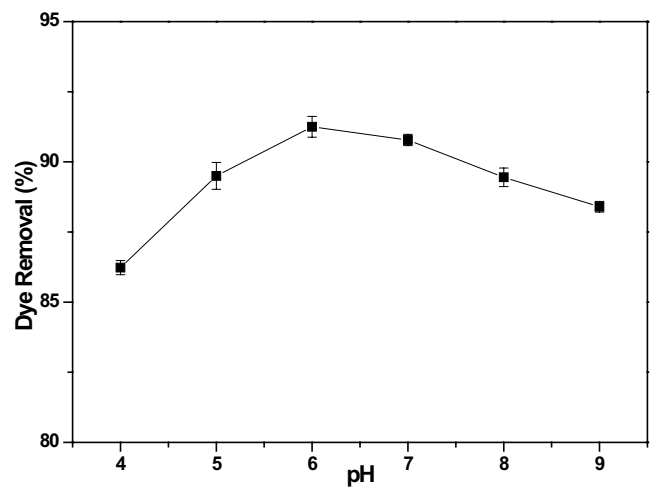


Fig. 11. Effect of solution pH on dye removal (initial concentration of dye = 5 mg/L, amount of MOF = 0.03 mg, and contact time = 24 h).

Here, C_e (mg/L) is the equilibrium concentration and Q_e (mg/g) is the amount of adsorbate adsorbed by the per unit mass of adsorbent. K_L and Q_L are the Langmuir constant related to rate of adsorption and adsorption capacity, respectively.

Equilibrium parameter R_L , a dimensionless constant and an essential characteristics of Langmuir isotherm, can be obtained by the following equation [58]:

$$R_L = \frac{1}{1 + K_L C_0} \quad (4)$$

where K_L is the Langmuir constant and C_0 (mg/L) is the highest dye concentration. The value of constant R_L provides the information about how favorable the adsorption process, that is, isotherm is favorable if value of R_L lies between 0 and 1, on other hand isotherm is unfavorable if $R_L > 1$, linear if $R_L = 1$, and irreversible if $R_L = 0$ [61].

3.7.3. Temkin adsorption isotherm

Temkin isotherm is presented by an equation [60]:

$$Q_e = \frac{RT}{b_T} \ln C_e + \frac{RT}{b_T} \ln K_T \tag{5}$$

The Temkin isotherm constants (b_T and K_T) can be calculated from slope and intercept of the plot of $\ln C_e$ vs. Q_e . K_T is the equilibrium binding constant (L/mg) corresponding to the maximum binding energy and constant b_T is related to the heat of adsorption. According to Temkin isotherm, there is a linear increase in the heat of adsorption of all the molecules with coverage of adsorbate over adsorbent surface [40].

Plots for the above three adsorption isotherm models viz. Freundlich, Langmuir, and Temkin were drawn using the experimental data (Figs. 12–14). Their corresponding constants are listed in Table 2. From Table 2, the Langmuir and Freundlich isotherm models revealed to be the best fit with the highest R^2 value (0.98709 and 0.98675, respectively). The value of $1/n$ obtained from the linear plot of Freundlich isotherm provides important information about the usability of the adsorbent over the concentration range of dye solution. In the present work, we found the value of $1/n$ to be 0.204 which made the Fe-BDC MOF adsorbent applicable for the entire range of CV dye concentration [61]. Similarly, the value of equilibrium parameter R_L , calculated using Eq. (4), is found to be 0.0038 suggesting the favorability of the isotherm [61].

3.8. Kinetics study

Three kinetics models, pseudo-first-order kinetics, pseudo-second-order kinetics, and intraparticle diffusion were applied to identify the mechanism that controls the overall removal rate in the adsorption process. Linear equations for these three models are expressed as [62,63]:

Pseudo-first-order kinetics:

$$\ln(Q_e - Q_t) = \ln Q_e - k_1 t \tag{6}$$

Pseudo-second-order kinetics:

$$\frac{t}{Q_t} = \frac{t}{Q_e} + \frac{1}{k_2 Q_e^2} \tag{7}$$

Intraparticle diffusion:

$$Q_t = k_i t^{1/2} + C \tag{8}$$

Here, Q_e (mg/g) and Q_t (mg/g) are the amount of dye adsorbed at equilibrium and at time t (min), respectively and k_1 (min^{-1}), k_2 ($\text{g}/\text{mg}\cdot\text{min}$), and k_i ($\text{mg}/\text{g}\cdot\text{min}^{1/2}$) are rate

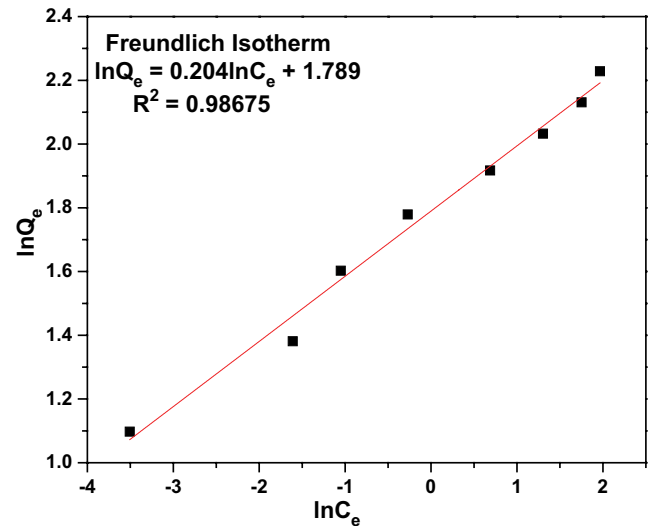


Fig. 12. Linear plot for Freundlich adsorption isotherm.

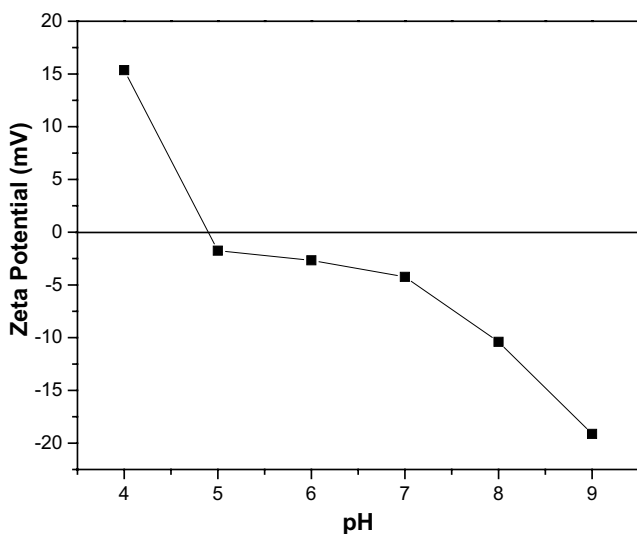


Fig. 11. Zeta potential of Fe-BDC MOF adsorbent.

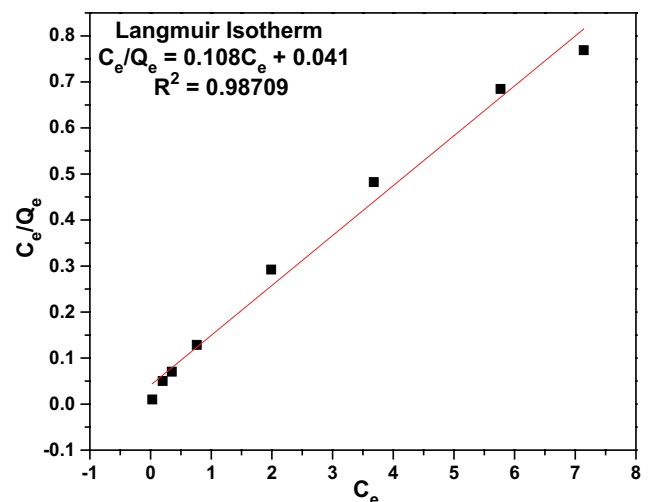


Fig. 13. Linear plot for Langmuir adsorption isotherm.

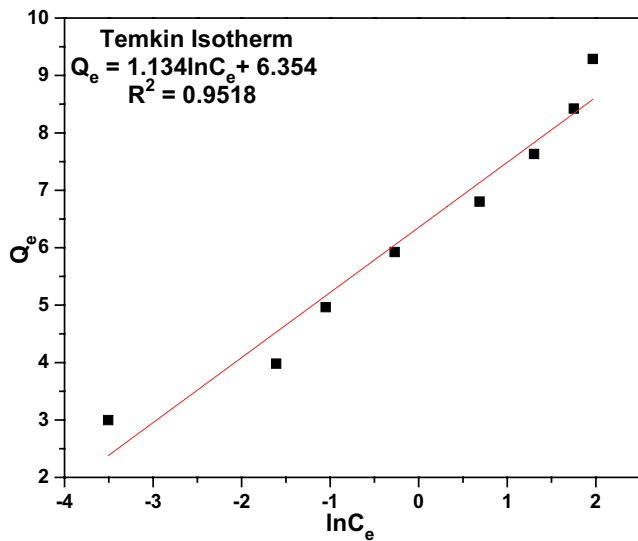


Fig. 14. Linear plot for Temkin adsorption isotherm.

constant of adsorption for pseudo-first-order, pseudo-second-order, and intraparticle diffusion, respectively. In intraparticle diffusion constant C reflects the boundary layer effect [62].

Three linear plots for the kinetic models are presented in Figs. 15–17 and their corresponding parameters are listed in Table 3. The value of R^2 (0.9954) for pseudo-second-order kinetics is closer to unity and is greater than that of the two other kinetic models. This suggests that the pseudo-second-order kinetic model with rate constant 1.22×10^{-2} g/mg.min is best fit for the present study. Further, the calculated uptake capacity ($Q_e^{cal} = 1.698$ mg/g) is in good agreement with the experimental uptake capacity ($Q_e^{exp} = 1.526$ mg/g). Therefore, we can conclude that removal of crystal violet dye from its aqueous solution proceeds via chemisorption process [63].

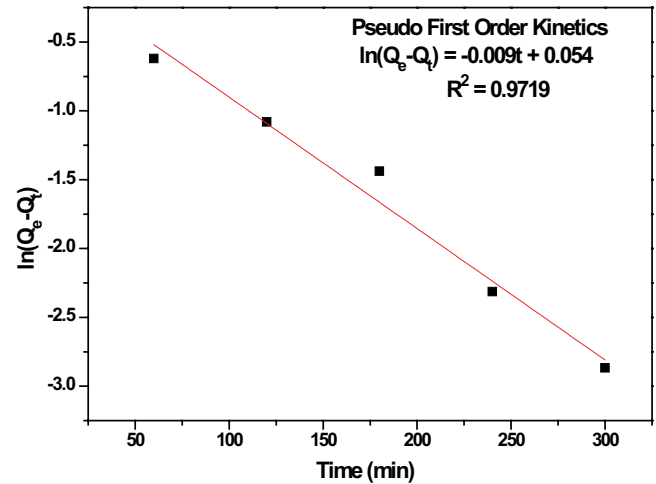


Fig. 15. Linear plot for pseudo-first-order kinetics.

3.9. Thermodynamic study

Study of effect of temperature on adsorption process provides important information about the free energy change, entropy change. We found an increase in adsorption capacity on increasing temperature that indicates the adsorption is endothermic and favorable at higher temperatures [32,64]. Spontaneity of the adsorption process can be determined with the help of thermodynamic parameters which were calculated by Van't Hoff equation [54,64]:

$$\ln \frac{Q_e}{C_e} = \frac{\Delta S}{R} - \frac{\Delta H}{RT} \tag{9}$$

The Gibb's free energy can be calculated by the following equation:

$$\Delta G = \Delta H - T\Delta S \tag{10}$$

Table 2
Isotherm parameters of crystal violet adsorption on Fe-BDC MOF

Concentration of dye (mg/L)		Q_e (mg/g)	Freundlich isotherm			Langmuir isotherm			Temkin isotherm		
C_0	C_e		n	K_f (mg/g)	R^2	Q_L (mg/g)	K_L (L/mg)	R^2	b_T	K_T (L/mg)	R^2
5	0	0.5									
10	0	1									
20	0	2									
30	0.03	2.997									
40	0.2	3.98									
50	0.35	4.965	4.902	5.983	0.98675	9.259	2.634	0.98709	2.185×10^3	271.895	0.9518
60	0.762	5.9238									
70	1.988	6.8012									
80	3.68	7.632									
90	5.769	8.4231									
100	7.14	9.286									

Cumulative adsorption capacity (for five cycles) has been calculated to be 36.3 mg/g using Freundlich isotherm model.

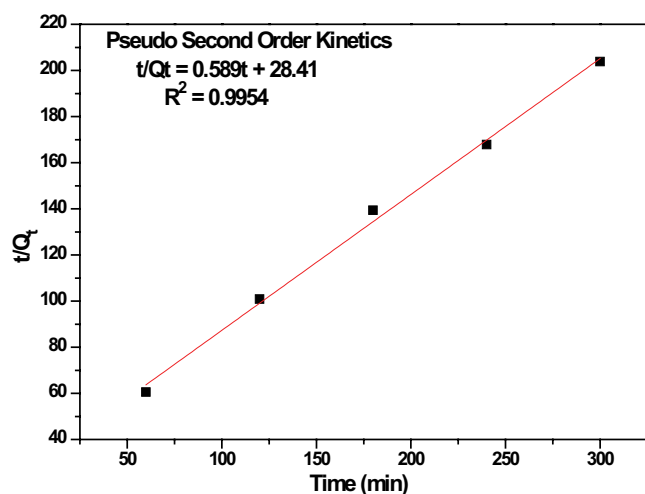


Fig. 16. Linear plot for pseudo-second-order kinetics.

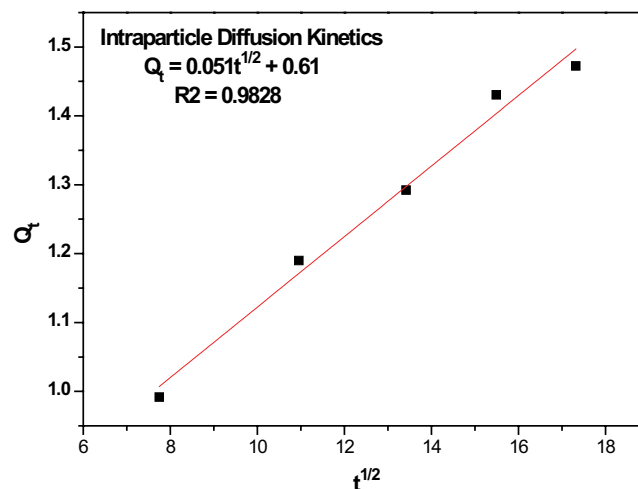


Fig. 17. Linear plot for intraparticle diffusion kinetics.

Table 3
Kinetics parameters of crystal violet adsorption on Fe-BDC MOF

Q_e (mg/g)	Pseudo-first-order			Pseudo-second-order			Intraparticle		
	Q_e (mg/g)	k_1 (min ⁻¹)	R^2	Q_e (mg/g)	k_2 (g/mg.min)	R^2	k_i (mg/g.min ^{1/2})	C	R^2
1.526 (5 mg/L)	1.055	0.009	0.9719	1.698	0.1221	0.9954	0.051	0.61	0.9828

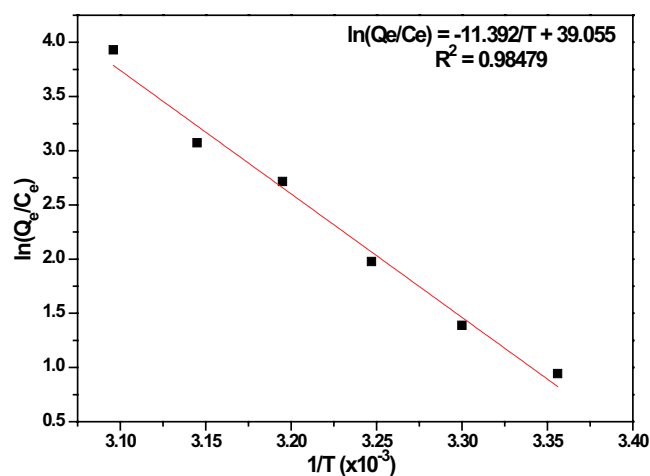
Here, ΔS (kJ/mol/K), ΔH (kJ/mol), and ΔG (kJ/mol) are the changes in entropy, enthalpy, and Gibb's free energy, respectively. C_e is the equilibrium concentration (mg/L) of dye solution, Q_e is the amount of dye adsorbed at equilibrium (mg/g), R is the gas constant (8.314 J/mol/K), and T is temperature (K). A straight line (Fig. 18) plotted between $\ln(Q_e/C_e)$ and $1/T$ can provide value of $\Delta H/R$ and $\Delta S/R$ as slope and intercept, respectively. Values of all thermodynamic parameters are listed in Table 4. An increase in randomness at the solid-solution interface during the adsorption is indicated by the positive value of ΔS . Endothermic process of adsorption is again confirmed by the positive value of ΔH . Further, negative value of ΔG suggests that the adsorption of CV dye on Fe-BDCMOF adsorbent is a spontaneous process. Decreasing value of ΔG with increasing temperature indicates that the adsorption is favorable at higher temperature [64].

3.10. Column adsorption study

The breakthrough curve and breakthrough parameters obtained by column adsorption study of CV dye removal using Fe-BDC MOF are shown in Fig. 19 and Table 5, respectively.

3.11. Dye desorption and reusability

Fig. 20 reveals the reusability of Fe-BDC MOF. Initially, in first cycle Fe-BDC MOF can remove 91% CV dye the removal capacity was reduced to 57% CV dye from its aqueous solution after five cycles. The adsorbed dye was recovered after sonication for 30 min in acidic medium. 98.85%

Fig. 18. Plot of $\ln(Q_e/C_e)$ vs. $1/T$ to give thermodynamic parameters.

dye could be recovered after first cycle which gradually reduced to 76% till 5th cycle (Table 6). The dye removal capacity of Fe-BDC MOF is 36.419 mg/g. The data reported in Table 6 reveals that the MOF can be effectively reused and the dye can be obtained to be reused as raw material in the industries.

Cost of preparation for 1 g of the MOF is 0.4 \$ in the laboratory. The cost will be much lower for conducting the pilot study. Moreover, the synthesized MOF can be reused several times and the dye can be recovered to be used as raw material for industries. So, use of Fe-BDC MOF for CV dye removal is cost-effective as well as environment friendly.

Table 4
Thermodynamic parameters for adsorption of CV on Fe-BDC MOF

Concentration (mg/L)	ΔH (kJ/mol)	ΔS (kJ/mol/K)	ΔG (kJ/mol) at temperatures					
			298 K	303 K	308 K	313 K	318 K	323 K
5	0.0947	0.325	-96.67	-98.29	-99.91	-101.54	-103.16	-104.78

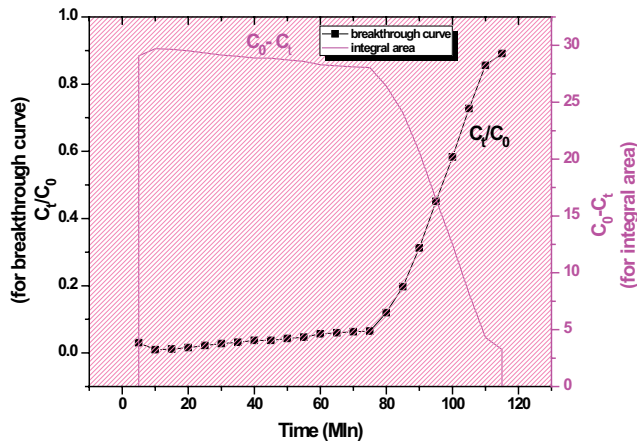


Fig. 19. Breakthrough curve of Fe-BDC MOF for CV dye removal.

Table 5
Breakthrough parameters for column adsorption study of CV dye using Fe-BDC MOF

Flow rate (mL/min)	2.5
Time (min)	115
Peak area (mg.min/L)	2,664.75
q_e (mg/g)	26.648
m_{total} (mg)	8.625
Q_{total} (mg)	6.662
R (%)	77.24

Here q_e is adsorption capacity, m_{total} is amount of dye loaded to the column, and Q_{total} is total dye adsorbed in column run.

4. Adsorption mechanism

To explain the adsorption mechanism between Fe-BDC MOF and CV dye SEM-EDX analysis of Fe-BDC MOF before and after adsorption were performed. As shown in Fig. 6 surface of adsorbent MOF is coated with a thick layer of CV dye. To further reveal the adsorption mechanism FT-IR analysis of the MOF before and after CV dye adsorption were also performed. It was found that the peak at $1,666\text{ cm}^{-1}$ disappeared after adsorption indicating Fe-BDC MOF successfully adsorbed the CV dye. Furthermore, the vibration stretching frequency of C=O band in Fe-BDC MOF was transferred from $1,589$ to $1,574\text{ cm}^{-1}$ which demonstrated that the presence of π - π interaction between the CV dye and Fe-BDC MOF has changed the electron cloud distribution of the molecule in the adsorption process. All observations confirm the π - π interaction between the CV

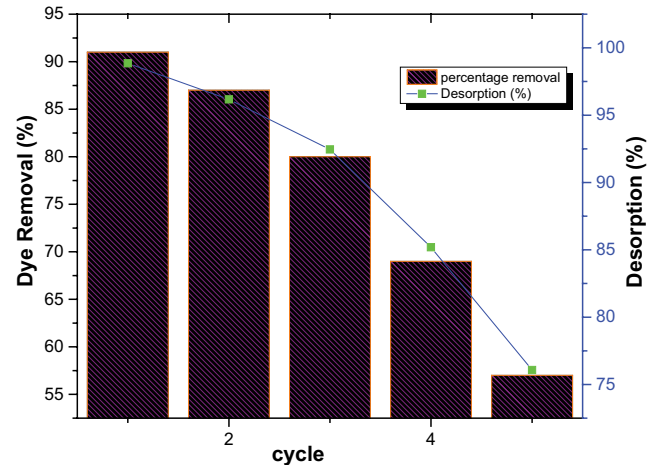


Fig. 20. CV dye adsorption and desorption efficiency of Fe-BDC MOF after five cycles and reusability.

dye and Fe-BDC MOF. A similar observation was reported by Duo et al. [65].

5. Comparison of adsorption of CV by Fe-BDC MOF with other adsorbents

The dye uptake capacity of Fe-BDC MOF for CV dye has been compared with various other adsorbents reported in the literature (Table 7). The result reveals that Fe-BDC MOF has higher dye adsorption capacity than that of other previously published adsorbents and can be used as a promising adsorbent for CV dye removal from its aqueous solution.

6. Economic appraisal

A rough assessment of the capital cost of using Fe-BDC MOF for CV was made based on the saturation capacity of the adsorbent alone, without considering other cost factors such as regeneration or spent adsorbent disposal cost. Adsorption system cost was judged as the relative cost for adsorbing 1 g of CV dye. Numerous researchers [71–73] have followed this procedure to calculate the adsorption process cost. Table 8 presents the economic cost and adsorption capacity of CV with other MOF adsorbents.

7. Conclusion

Fe-BDC MOF showed 100% removal of crystal violet dye from its aqueous solution with an initial concentration of 5 mg/L and removal of the dye decreases with increasing concentration. Maximum adsorption capacity was found to

Table 6
Dye adsorption, desorption, and reusability of MOF and dye

No. of cycles	Dye adsorption (%)	Dye desorption (%)	Dye removal per cycle (mg/g)	Cumulative dye removal capacity (mg/g)
1	91	98.85	9.267	
2	87	96.17	8.062	
3	80	92.45	7.414	36.419
4	69	85.19	6.394	
5	57	76.07	5.282	

Table 7
Comparison with other adsorbents for the removal of CV dye

S. No.	Adsorbent	Dye uptake capacity (mg/g)	Reference
1	<i>Acesia nilotica</i> leaves	33	[41]
2	Citric acid modified pea peel	17.6	[46]
3	<i>Chenopodium album</i> ash	9.42	[55]
4	Jute fiber carbon	27.99	[66]
5	Orange peel	6.1	[67]
6	Banana peel	7.9	[67]
7	<i>Cucumis sativa</i> fruit peel	34.24	[68]
8	Bagasse fly ash	26.233	[69]
9	<i>Agaricus bisporous</i>	21.74	[70]
10	Fe-BDC MOF	36.419	Present study

Table 8
Cost and adsorption (saturation) capacity of Fe-BDC MOF in comparison with other adsorbents for adsorption of CV

Adsorbent	Saturation capacity (mg/g)	Price/g of adsorbent compared to Fe-BDC MOF price	Price/adsorbed g of CV compared to Fe-BDC MOF price	Reference
Fe-BDC MOF	36.419	1	1	Present work
Cu ₃ (BTC) ₂	0.29	13.83	1,736.30	29
H ₂ dtoaCu	165.83	18.87	4.14	28
IFMC-2	2.4	28.28	429.19	30

be 9.286 mg/g in one cycle when 0.1 g of adsorbent is added to the dye solution having initial concentration 100 mg/L which has been improved to 36.42 g in batch adsorption experiment. Adsorption capacity of Fe-BDC MOF has been recorded 26.65 mg/g for column method. Freundlich and Langmuir adsorption isotherm and pseudo-second-order kinetic model reveal good applicability for the study of interaction between the dye and Fe-BDC MOF. Freundlich isotherm suggests the Fe-BDC MOF can remove CV dye from its aqueous solution over its entire concentration range. Removal of the dye by adsorption on Fe-BDC MOF is favorable at higher temperature range. Thermodynamic parameters reveal endothermic, spontaneous adsorption in which there is an increase in randomness at the solid-solution interface during the process. The adsorbed dye can be recovered to be used as raw material for industries. MOF has also been regenerated for removal of crystal violet with significant efficiency upto five cycles. Fe-BDC MOF

developed in the present study is economic in comparison to several MOF viz. Cu₃(BTC)₂, H₂dtoaCu, and IFMC-2.

Acknowledgments

Authors are thankful to Dr. Pranaw Kumar and Head Fuel Chemistry Division, Bhabha Atomic Research Centre, Mumbai, India for recording BET surface area and pore volume. Mr. Sanju Soni is thankful to UGC and Guru Ghasidas University for VRET fellowship.

References

- [1] A. Elsagh, O. Moradi, A. Fakhri, F. Najafi, R. Alizadeh, V. Haddafi, Evaluation of the potential cationic dye removal using adsorption by grapheme and carbon nanotubes as adsorbents surfaces, *Arabian J. Chem.*, 10 (2017) S2862–S2869.
- [2] Z.H. Farahani, H.H. Monfared, N.M. Mahmoodi, Graphene oxide nanosheet: preparation and dye removal from binary

- system colored wastewater, *Desal. Water Treat.*, 56 (2015) 2382–2394.
- [3] A. Mittal, A. Malviya, D. Kaur, J. Mittal, L. Kurup, Studies on the adsorption kinetics and isotherms for the removal and recovery of methyl orange from wastewaters using waste materials, *J. Hazard. Mater.*, 148 (2007) 229–240.
 - [4] S. Chen, J. Zhang, C. Zhang, Q. Yue, Y. Li, C. Li, Equilibrium and kinetics studies of methyl orange and methyl violet adsorption on activated carbon derived from *phragmites australis*, *Desalination*, 252 (2010) 149–156.
 - [5] V.K. Gupta, Suhas, Application of low-cost adsorbents for dye removal – a review, *J. Environ. Manage.*, 90 (2009) 2313–2342.
 - [6] L. Bulgariu, L.B. Escudero, O.S. Bello, M. Iqbal, J. Nisar, K.A. Adegoke, F. Alakhras, M. Kornaros, I. Anastopoulos, The utilization of leaf-based adsorbents for dyes removal: a review, *J. Mol. Liq.*, 276 (2019) 728–747.
 - [7] A. Kausar, M. Iqbal, A. Javed, K. Aftab, Z.-i.-H. Nazil, H.N. Bhatti, S. Nouren, Dye adsorption using clay and modified clay: a review, *J. Mol. Liq.*, 256 (2018) 395–407.
 - [8] I. Anastopoulos, A. Hosseini-Bandegharai, J. Fu, A.C. Mitropoulos, G.Z. Kyzas, Use of nanoparticles to dye adsorption: review, *J. Dispersion Sci. Technol.*, 39 (2017) 836–847.
 - [9] A. Bhatnagar, M. Sillanpää, A. Wittek-Krowiak, Agricultural waste peels as versatile biomass for water purification – a review, *Chem. Eng. J.*, 270 (2015) 244–271.
 - [10] I. Khurana, A. Saxena, Bharti, J.M. Khurana, P.K. Rai, Removal of dyes using Graphene-based composites: a review, *Water Air Soil Pollut.*, 228 (2017) 180, doi: 10.1007/s11270-017-3361-1.
 - [11] B. Tanhaei, A. Ayati, M. Lahtinen, M. Sillanpää, Preparation and characterization of a novel chitosan/Al₂O₃/magnetite nanoparticles composite adsorbent for kinetic, thermodynamic and isotherm studies of Methyl Orange adsorption, *Chem. Eng. J.*, 259 (2015) 1–10.
 - [12] S.I. Siddiqui, F. Zohra, S.A. Chaudhry, *Nigella sativa* seed based nanohybrid composite-Fe₃O₄-SnO₂/BC: a novel material for enhanced adsorptive removal of methylene blue from water, *Environ. Res.*, 178 (2019) 108667, doi: 10.1016/j.envres.2019.108667.
 - [13] A.M. Hameed, Synthesis of Si/Cu amorphous adsorbent for efficient removal of methylene blue dye from aqueous media, *J. Inorg. Organomet. Polym.*, 30 (2020) 2881–2889.
 - [14] A.M. Osman, A.H. Hendi, T.A. Saleh, Simultaneous adsorption of dye and toxic metal ions using an interfacially polymerized silica/polyamide nanocomposite: kinetic and thermodynamic studies, *J. Mol. Liq.*, 314 (2020) 113640, doi: 0.1016/j.molliq.2020.113640.
 - [15] K.Y. Andrew Lin, H.A. Chen, C.J. Hsu, Iron-based metal organic framework, MIL-88A, as a heterogeneous persulfate catalysis for decolorization of rhodamine B in water, *RSC Adv.*, 5 (2015) 32520–32530.
 - [16] C.Y. Sun, X.L. Wang, C. Qin, J.L. Jin, Z.M. Su, P. Huang, K.Z. Shao, Solvatochromic behaviour of chiral mesoporous metal-organic frameworks and their applications for sensing small molecules and separating cationic dyes, *Chem. Eur. J.*, 19 (2013) 3639–3645.
 - [17] S. Soni, P.K. Bajpai, C. Arora, A review on metal organic framework: synthesis, properties and application. *Charact. Appl. Nanomater.*, 2 (2019) 1–20, doi: 10.24294/can.v2i1.551
 - [18] H. Guo, F. Lin, J. Chen, F. Li, W. Weng, Metal-organic framework MIL-125(Ti) for efficient adsorptive removal of rhodamine B from aqueous solution, *Appl. Organomet. Chem.*, 29 (2015) 12–19.
 - [19] S. Kumar, G. Verma, W.Y. Gao, Z. Niu, L. Wojtas, S. Ma, Anionic metal-organic framework for selective dye removal and CO₂ fixation, *Eur. J. Inorg. Chem.*, 2016 (2016) 4373–4377.
 - [20] E. Haque, J.E. Lee, I.T. Jang, Y.K. Hwang, J.S. Chang, J. Jegal, S.H. Jung, Adsorptive removal of methyl orange from aqueous solution with metal-organic frameworks, porous chromium benzenedicarboxylates, *J. Hazard. Mater.*, 181 (2010) 535–542.
 - [21] E. Haque, J.W. Jun, S.H. Jung, Adsorptive removal of methyl orange and methylene blue from aqueous solution with a metal-organic framework material, iron terephthalate (MOF-235), *J. Hazard. Mater.*, 185 (2011) 507–511.
 - [22] S. Soni, P.K. Bajpai, J. Mittal, C. Arora, Utilisation of cobalt doped Iron based MOF for enhanced removal and recovery of methylene blue dye from waste water, *J. Mol. Liq.*, 314 (2020) 113642, doi: 10.1016/j.molliq.2020.113642.
 - [23] M.A. Nazir, N.A. Khan, C. Cheng, S.S.A. Shah, T. Najam, M. Arshad, A. Sharif, S. Akhtar, A.U. Rehman, Surface induced growth of ZIF-67 at Co-layered double hydroxide: removal of methylene blue and methyl orange from water, *Appl. Clay Sci.*, 190 (2020) 105564, doi: 10.1016/j.clay.2020.105564.
 - [24] X. Liu, C. Hao, L. Cui, Y. Wang, An anionic cadmium-organic framework with an uncommon 3,3,4,8-c network for efficient organic dye separation, *Polyhedron*, 188 (2020) 114685, doi: 10.1016/j.poly.2020.114685.
 - [25] N. Marsiezade, V. Javanbakht, Novel hollow beads of carboxymethyl cellulose/ZSM-5/ZIF-8 for dye removal from aqueous solution in batch and continuous fixed bed systems, *Int. J. Biol. Macromol.*, 162 (2020) 1140–1152.
 - [26] Q. He, Q. Chen, M. Lü, X. Liu, Adsorption behavior of rhodamine B on UiO-66, *Chin. J. Chem. Eng.*, 22 (2014) 1285–1290.
 - [27] M.S. Embaby, S.D. Elwany, W. Setyaningsih, M.R. Saber, The adsorptive properties of UiO-66 towards organic dyes: a record adsorption capacity for the anionic dye alizarin red S, *Chin. J. Chem. Eng.*, 26 (2017) 731–739.
 - [28] X. Li, J.L. Zheng, L. Huang, O. Zheng, Z. Lin, L. Guo, B. Qiu, G. Chen, Adsorption removal of crystal violet from aqueous solution using a metal-organic frameworks material, copper coordination polymer with dithiooxamide, *J. Appl. Polym. Sci.*, 129 (2013) 2857–2864.
 - [29] S. Loera-Serna, J. Garcia-Ortiz, E. Ortiz, Dyes adsorption on Cu₃(BTC)₂ metal-organic framework, *Adv. Mater.: TechConnect Briefs*, 1 (2016) 331–334.
 - [30] J.S. Qin, S.R. Zhang, D.Y. Du, P. Shen, S.J. Bao, Y.Q. Lan, Z.M. Su, A microporous anionic metal-organic framework for sensing luminescence of lanthanide(III) ions and selective absorption of dyes by ionic exchange, *Chem. Eur. J.*, 20 (2014) 5625–5630.
 - [31] J. Zhang, F. Li, Q. Sun, Rapid and selective adsorption of cationic dyes by a unique metal-organic framework with decorated pore surface, *Appl. Surf. Sci.*, 440 (2018) 1219–1226.
 - [32] A. Mohamed, T.A. Osman, M.S. Toprak, M. Muhammed, A. Uheida, Surface functionalized composite nanofibers for efficient removal of arsenic from aqueous solutions, *Chemosphere*, 180 (2017) 108–116.
 - [33] A. Mohamed, S. Yousef, M.A. Abdelnaby, T. Osman, B. Hama-wandi, M. Toprak, M. Muhammed, A. Uheida, Photocatalytic degradation of organic dyes and enhanced mechanical properties of PAN/CNTs composite nanofibers, *Sep. Purif. Technol.*, 182 (2017) 219–223.
 - [34] S. Kuriakose, B. Satpati, S. Mohapatra, Highly efficient photocatalytic degradation of organic dyes by Cu doped ZnO nanostructures, *Phys. Chem. Chem. Phys.*, 17 (2015) 25172–25181.
 - [35] M.A. Habib, M. Muslim, M.T. Shahadat, M.N. Islam, I.M.I. Ismail, T.S.A. Islam, A.J. Mahmood, Photocatalytic decolourization of crystal violet in aqueous nano-ZnO suspension under visible light irradiation, *J. Nanostruct. Chem.*, 3 (2013) 70, doi: 10.1186/2193-8865-3-70.
 - [36] M.N. Khan, O. Bashir, T.A. Khan, S.A. Al-Thabaiti, Z. Khan, Catalytic activity of cobalt nanoparticles for dye and 4-nitro phenol degradation: a kinetic and mechanistic study, *Int. J. Chem. Kinet.*, 49 (2017) 438–454.
 - [37] M.N. Khan, O. Bashir, T.A. Khan, S.A. Al-Thabaiti, Z. Khan, CTAB capped synthesis of bio-conjugated silver nanoparticles and their enhanced catalytic activities, *J. Mol. Liq.*, 258 (2018) 133–141.
 - [38] M. Pourgholi, R.M. Jahandizi, M. Miranzadeh, O.H. Beigi, S. Dehghan, Removal of dye and COD from textile wastewater using AOP (UV/O₃, UV/H₂O₂, O₃/H₂O₂ and UV/H₂O₂/O₃), *J. Environ. Health Sustainable Dev.*, 3 (2018) 630–636.
 - [39] J.J. Pignatello, E. Oliveros, A. Mackay, Advanced oxidation processes for organic contaminant destruction based on the Fenton reaction and related chemistry, *Crit. Rev. Environ. Sci. Technol.*, 36 (2006) 1–84.

- [40] A. Mittal, J. Mittal, A. Malviya, D. Kaur, V.K. Gupta, Adsorption of hazardous dye crystal violet from waste water by waste materials, *J. Colloid Interface Sci.*, 343 (2010) 463–473.
- [41] A.L. Prasad, T. Santhi, Adsorption of hazardous cationic dyes from aqueous solution onto *Acacia nilotica* leaves as an eco friendly adsorbent, *Sustainable Environ. Res.*, 22 (2012) 113–122.
- [42] S. Senthilkumar, P. Kalaamani, C.V. Subburaam, Liquid phase adsorption of crystal violet onto activated carbons derived from male flowers of coconut tree, *J. Hazard. Mater.*, 136 (2006) 800–808.
- [43] C. Arora, S. Soni, S. Sahu, J. Mittal, P. Kumar, P.K. Bajpai, Iron based metal organic framework for efficient removal of methylene blue dye from industrial waste, *J. Mol. Liq.*, 284 (2019) 343–352.
- [44] S. Choudhury, S. Chakraborty, P.D. Saha, Removal of crystal violet from aqueous solution by adsorption onto eggshells: equilibrium, kinetics, thermodynamics and artificial neural network modelling, *Waste Biomass Valorization*, 4 (2012) 655–664.
- [45] A. Mittal, J. Mittal, A. Malviya, D. Kaur, V.K. Gupta, Decoloration treatment of a hazardous triarylmethane dye, light green SF (yellowish) by waste material adsorbents, *J. Colloid Interface Sci.*, 342 (2010) 518–527.
- [46] T.A. Khan, R. Rahman, E.A. Khan, Decolorization of bismarck brown R and crystal violet in liquid phase using modified pea peels: non-linear isotherm and kinetics modelling, *Model. Earth Syst. Environ.*, 2 (2016) 1–11.
- [47] A. Ikhlaq, H.M.S. Munir, A. Khan, F. Javed, K.S. Joya, Comparative study of catalytic ozonation and Fenton-like processes using iron-loaded rice husk ash as catalyst for the removal of methylene blue in wastewater, *Ozone Sci. Eng.*, 41 (2018) 250–260.
- [48] H.M.S. Munir, N. Feroze, A. Ikhlaq, M. Kazmi, F. Javed, H. Mukhtar, Removal of colour and COD from paper and pulp industry wastewater by ozone and combined ozone/UV process, *Desal. Water Treat.*, 137 (2019) 154–161.
- [49] V.K. Gupta, Suhas, I. Tyagi, S. Agarwal, R. Singh, M. Chaudhary, A. Harit, S. Kushwaha, Column operation studies for the removal of dyes and phenols using a low cost adsorbent, *Global J. Environ. Sci. Manage.*, 2 (2016) 1–10.
- [50] K. Tan, N. Nijem, P. Canepa, Q. Gong, J. Li, T. Thonhauser, Y.J. Chabal, Stability and hydrolyzation of metal-organic frameworks with paddle wheel SBUs upon hydration, *Chem. Mater.*, 24 (2012) 3153–3167.
- [51] X. Zhao, S. Liu, Z. Tang, H. Niu, Y. Cai, W. Meng, F. Wu, J.P. Giesy, Synthesis of magnetic metal organic framework (MOF) for efficient removal of organic dyes from water, *Sci. Rep.*, 5 (2015) 11849, doi: 10.1038/scep11849.
- [52] Z. Cheng, J. Liao, B. He, F. Zhang, F. Zhang, X. Huang, L. Zhou, One step fabrication of grapheme oxide enhanced magnetic composite for highly efficient dye adsorption and catalysis, *ACS Sustainable Chem. Eng.*, 2015 (2015) 1677–1685.
- [53] Z. Eren, F.N. Acrar, Adsorption of reactive black 5 from an aqueous solution: equilibrium and kinetics studies, *Desalination*, 194 (2006) 1–10.
- [54] H. Singh, Samiksha, S. Roohi, Removal of basic dyes from aqueous solutions using mustard waste ash and buffalo dung ash, *Int. J. Environ. Sci.*, 3 (2013) 1711–1725.
- [55] C. Arora, D. Sahu, D. Bharti, V. Tamrakar, S. Soni, S. Sharma, Adsorption of hazardous dye crystal violet from industrial waste using low-cost adsorbent *Chenopodium album*, *Desal. Water Treat.*, 167 (2019) 324–332.
- [56] K. Zare, H. Sadege, R.S. Ghoshekandi, B. Maazinejad, V. Ali, I. Tyagi, S. Agarwal, V.K. Gupta, Enhanced removal of toxic congo red dye using multi walled carbon nanotubes: kinetic, equilibrium studies and its comparison with other adsorbents, *J. Mol. Liq.*, 212 (2015) 266–271.
- [57] A. Mittal, J. Mittal, A. Malviya, V.K. Gupta, Removal and recovery of chrysoidine Y from aqueous solutions by waste materials, *J. Colloid Interface Sci.*, 344 (2010) 497–507.
- [58] B.H. Hameed, A.A. Ahmad, Batch adsorption of methylene blue from aqueous solution by garlic peel, an agricultural waste biomass, *J. Hazard. Mater.*, 164 (2009) 870–875.
- [59] P. Qin, Y. Yang, X. Zhang, J. Niu, H. Yang, S. Tian, J. Zhu, M. Lu, Highly efficient, rapid and simultaneous removal of cationic dyes from aqueous solution using monodispersed mesoporous silica nanoparticles as the adsorbent, *Nanomaterials*, 8 (2018) 4, doi: 10.3390/nano801004.
- [60] Y. Xu, J. Jin, X. Li, Y. Han, H. Meng, C. Song, X. Zhang, Magnetization of a Cu(II)-1,3,5-benzenetricarboxylate metal-organic framework for efficient solid phase extraction of Congo red, *Microchim. Acta*, 182 (2015) 2313–2320.
- [61] B.S. Kaith, J. Sharma, Sukriti, S. Sethi, T. Kaur, U. Shankar, V. Jassal, Fabrication of green device for efficient capture of toxic methylene blue from industrial effluent based on $K_2Zn_2(Fe(CN)_{6.2}) \cdot 9H_2O$ nanoparticles reinforced gum xanthan-psyllium hydrogel nanocomposite, *J. Chin. Adv. Mater. Soc.*, 4 (2016) 249–268.
- [62] A.K. Kushwaha, N. Gupta, M.C. Chattopadhyaya, Removal of cationic methylene blue and malachite green dyes from aqueous solution by waste materials of *Daucus carota*, *J. Saudi Chem. Soc.*, 18 (2014) 200–207.
- [63] X. Li, L. Zheng, L. Huang, O. Zheng, Z. Lin, L. Guo, B. Qiu, G. Chen, Adsorption removal of crystal violet from aqueous solution using a metal organic frameworks material, copper coordination polymer with dithiooxamide, *J. Appl. Polym. Sci.*, 129 (2013) 2857–2864.
- [64] C. Li, X. Wang, D. Meng, L. Zhou, Facile synthesis of low cost magnetic biosorbent from peach gum polysaccharide for selective and efficient removal of cationic dyes, *Int. J. Biol. Macromol.*, 107 (2018) 1871–1878.
- [65] H. Duo, H. Tang, J. Ma, X. Lu, L. Wang, X. Liang, Iron-based metal-organic framework as an effective sorbent for the rapid and efficient removal of illegal dyes, *New J. Chem.*, 43 (2019) 15351–15358.
- [66] K. Porkodi, K. Vasanth Kumar, Equilibrium, kinetics and mechanism modeling and simulation of basic and acid dyes sorption onto jute fiber carbon: eosin yellow, malachite green and crystal violet single component systems, *J. Hazard. Mater.*, 143 (2007) 311–327.
- [67] G. Annadurai, R.S. Juang, D.J. Lee, Use of cellulose-based wastes for adsorption of dyes from aqueous solutions, *J. Hazard. Mater.*, 92 (2004) 263–274.
- [68] T. Smitha, S. Thirumalisamy, S. Manonmani, Equilibrium and kinetics study of adsorption of crystal violet onto the peel of *Cucumis sativa* fruit from aqueous solution, *Electron. J. Chem.*, 9 (2012) 1091–1101.
- [69] I.D. Mall, V.C. Srivastava, N.K. Agarwal, Removal of orange-G and methyl violet dyes by adsorption onto bagasse fly ash kinetic study and equilibrium isotherm analysis, *Dyes Pigment.*, 69 (2006) 210–223.
- [70] P. Pandey, R.P. Singh, K.N. Singh, P. Manisankar, Evaluation of the individuality of white rot macro fungus for the decolorization of synthetic dye, *Environ. Sci. Pollut. Res.*, 20 (2012) 238–249.
- [71] M.-H. Baek, C.O. Ijagbemi, S.-J. O, D.-S. Kim. Removal of Malachite Green from aqueous solution using degreased coffee bean, *J. Hazard. Mater.*, 176 (2010) 820–828.
- [72] B.H. Hameed, M.I. El-Khaiary, Batch removal of malachite green from aqueous solutions by adsorption on oil palm trunk fibre: equilibrium isotherms and kinetic studies, *J. Hazard. Mater.*, 154 (2008) 237–244.
- [73] R. Malik, D.S. Ramteke, S.R. Wate, Adsorption of malachite green on groundnut shell waste based powdered activated carbon, *Waste Manage.*, 27 (2007) 1129–1138.